La mer 31: 107-116, 1993
Société franco-japonaise d'océanographie, Tokyo

# A numerical simulation of the general circulation in the world ocean

## Part 1. Temperature and velocity fields*

Chitose ARAKAWA** and Kenzo TAKANO**

**Abstract:** A numerical simulation is carried out for an annual cycle of the general circulation in the world ocean. The model ocean extends form 70°S to 70°N. The Arctic Ocean and ice phase are ignored. Salinity is assumed to be a constant. The grid size is 2° in longitude and latitude. The circulation is driven by a prescribed surface wind stress and a surface heat flux assumed to be proportional to the difference between the predicted sea surface temperature and a prescribed reference atmospheric temperature. The external forcing varies with a period of one year. Compared with observations, the simulated sea surface temperature is a little high at high latitudes in both hemispheres, and isotherms are not well concentrated in the Kuroshio and Gulf Stream regions. However, its major features agree well with observations. The so-called "Orient Express" ("Indian Ocean Express") is identified by subsurface isotherms. The Agulhas Retroflection cleary appears in the temperature, velocity and stream function for the transport. The Indonesian Throughflow may not be well simulated; in July-August it flows from the Indian Ocean to the Pacific Ocean. The transport of the Antarctic Circumpolar Current is compatible with observations, but the subtropical gyre extends to the north too much in the northern hemisphere.

### 1. Introduction

The purpose of the present study is to understand the mechanism for the ocean heat transport and its annual cycle in the global ocean, Pacific Ocean, Indian Ocean and Atlantic Ocean by use of an ocean circulation model.

The world ocean circulation is a key factor governing not only the global water mass dsitribution but also the global climate change through the ocean surface temperature which depends, to a great extent, on the ocean heat transport.

The circulation in the model ocean is driven by a wind stress and a surface heat flux. The external forcing is given by climatological data and varies with a period of one year.

Part 1 describes the temperature and velocity fields. A separate paper will present Part 2 which describes the meridional and interoceanic heat transports.

* Received March 18, 1993
** School of Environmental Sciences, University of Tsukuba, Tsukuba 305

### 2. Model

The grid structure and the finite differencing are the same as those described in papers by TAKANO (1974, 1986). The model world ocean extends from 70°N to 70°S. The maximum water depth is 5000m. The Arctic Ocean is excluded. Five levels are set up in the vertical. The horizontal components of velocity are calculated at depths of 20, 280, 720, 1300 and 3100m. The vertical component of velocity is calculated at depths of 150, 500, 1010 and 2200m. The ocean depth is either of these four depths or 5000m. The grid size is 2° in longitude and latitude. The ocean geometry given by DBDB5 (National Geophysical Data Center, 1986) is approximated with this grid. Apart from the main landmass comprising Eurasia, Africa and the Americas, there are seven separate landmasses: the Antarctica, Madagascar, Australia, New Guinea, New Zealand, Japan, Iceland and England-Ireland. The coastlines are defined by points where the temperature and the vertical component of velocity are defined. Ice phase is ignored. Salinity is assumed to be a constant of 35‰ everywhere. The water density

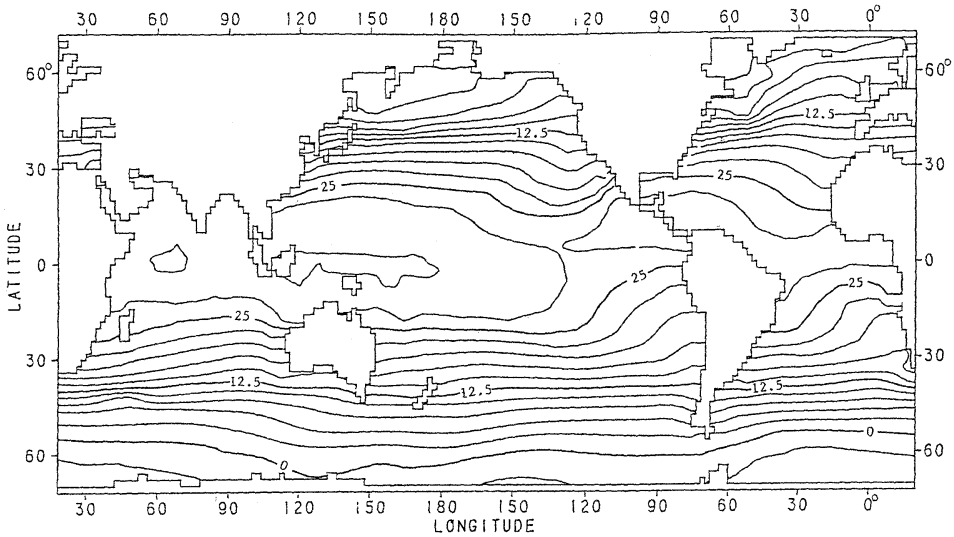


Fig. 1. Reference atmospheric temperature (°C). Annual average.

is calculated as a function of temperature and depth with a formula of FRIEDRICH and LEVITUS (1972).

The momentum advection is neglected, because the grid size is too wide for the momentum advection to be significant.

Simple, conventional closure schemes are used for approximating subgrid scale diffusion of momentum and heat, except for vertical diffusion of heat. Instantaneous complete mixing of heat occurs over the unstable parts of the water column whenever the vertical stratification becomes unstable.

The horizontal velocity vanishes at the lateral boundary. The bottom friction ($\tau_x$, $\tau_y$) is calculated by assuming the presence of the bottom Ekman layer:

$$\tau_x = \rho\sqrt{|f|k/2}\,(u \mp v),\quad \tau_y = \sqrt{|f|k/2}\,(\pm u + v)$$

where $\rho$ is the water density, $k$ the coeffcieint of vertical diffusion, $f$ the Coriolis parameter, $u$ and $v$ the eastward and northward components of velocity at the lowermost level, the upper signs refer to the northern hemisphere and the lower signs refer to the southern hemisphere.

The vertical component of velocity vanishes at the surface (rigid-lid approximation).

At the surface, the vertical shear of the horizontal velocity is specified by a given surface wind stress. Monthly climatological wind stress data (HELLERMAN and ROSENSTEIN, 1983) on a grid of $2° \times 2°$ are used.

There is no heat flux across the lateral and lower boundaries. The surface heat flux $Q$ is made proportional to the difference between a specified reference atmospheric temperature $T_a$ and the predicted temperature $T_1$ at the uppermost level:

$$Q = \rho c d\,(T_a - T_1) \qquad (1)$$

with a constant of proportionality $d$ and the specific heat $c$.

The reference atmospheric temperature is determined as follows. Formula (1) gives

$$T_a = T_1 + Q/(\rho c d)$$

where monthly data by ESBENSEN and KUSHNIR (1981) are used for $Q$ and $T_1$. Although $d$ varies to some degree with time, longitude and latitude, a constant of 30 W/m$^2$ is assumed. Since their data are given on a grid of $4° \times 4°$, linear interpolation is done to define $T_a$ on a grid of $2° \times 2°$. Figure 1 shows the annual average of $T_a$. The space and time average of $T_a$ is 18.25 ℃ in the Indian Ocean, 19.99° C in the Pacific Ocean, and 17.70° C in the Atlantic Ocean. Between 70° S and 38° S the time-average of $T_a$ is highest in the Pacific Ocean, between 38° S and 24° S it is highest in the Indian Ocean, and to the north of 24° S it is highest in the Atlantic Ocean.

The rigid-lid approximation breaks down the horizontal velocity into two components; one is the barotropic component (vertical average) and the other is the baroclinic component (deviation from the vertical average). While there is no interaction between both components of velocity through the momentum advection which is neglected here, there is through the combined effect of the pressure and depth gradient at the bottom, and through the heat advection.

Equation of continuity allows to introduce the stream function for the barotropic component of velocity multiplied by the water depth. The stream function is obtained by solving a vorticity equation. Hole relaxation technique (TAKANO, 1974) is used for determining the value of the stream function on the coast of each separate landmass (transport between landmasses).

The numerical computation consists of three phases. In Phase 1, the grid size is 4° in longitude and latitude. The coefficient of horizontal diffusin is $10^6 m^2/s$ for momentum, and $5\times10^4$ $m^2/s$ for heat. The coefficient of vertical diffusion is $10^{-4}m^2/s$ for momentum and heat. The annual averages of the wind stress and the reference atmospheric temperature are applied. With a time step of 6 hours, the momentum equations are integrated over 120 years from an initial state where there is no motion and the temperature varies with latitude and depth. Since a time step of 60 hours is applied to the thermal equation and a time step of 36 minutes to the vorticity equation, the simulated time is 1200 years for the thermal equation and 12 years for the vorticity equation.

In Phase 2, the grid size is reduced to 2° in longitude and latitude. The coefficient of horizontal diffusion is reduced to $10^5 m^2/s$ for the momentum and to $2.5\times10^3 m^2/s$ for the heat, but the coefficients of vertical diffusion remain unchanged. A large coefficient is required for momentum to suppress computational noise of checkerboard pattern (TAKANO, 1975). Starting from the final state in Phase 1, the time integration is forwarded for 12 years. A time step of 3 hours is applied to the momentum and thermal equations, while a time step of 22.5 minutes is applied to the vorticity equation. The external forcing remains constant in time.

Table 1. Values of $d$, $k$ and $A$ (coefficient of horizontal diffusion of heat)

| Case | $d(W/m^2K)$ | $k(10^{-4}m^2/s)$ | $A(10^3m^2/s)$ |
|---|---|---|---|
| 1 | 30 | 1.0 | 2.5 |
| 2 | 30 | 1.0 | 1.0 |
| 3 | 60 | 1.0 | 1.0 |
| 4 | 60 | 0.3 | 1.0 |

In Phase 3, the external forcing varies with a period of one year. Starting from the final state in Phase 2, the time integration is synchronously carried out over 42 years with the same time steps as in Phase 2. Since the time step for the vorticity equation is 1/8 of that for the other equations, the voriticity equation is integrated 8 times more than the momentum and thermal equations. Interannual variability still remains but is very small. While this case is hereafter referred to as Case 1, three additional cases, Cases 2 to 4, with different parameter values shown in Table 1 are dealt with for examining to what extent the result depends on the choice of them. The coefficient of horizontal diffusion of momentum is $10^5 m^2/s$ in any case. Additional time integration is forwarded for about 50 years in each case. The output from Case 1 will be outlined unless otherwise mentioned.

The velocity and temperature snapshots are saved every 10 days over the last one year. These 36 sets of data are analyzed. Studies with these data sets are reported in other papers (ARAKAWA and TAKANO, 1991; TAKANO, 1992a).

## 3. Temperature field

Figure 2 shows the annual average of the simulated sea surface temperature (SST), which is compared with seasonal data compiled by NODC/NOAA (1983), hereafter referred to as NOAAT. Since NOAAT are given on a grid of $1°\times1°$, they are averaged on an area of $2°\times2°$ for comparing the both with 2° resolution. The general aspect agrees well with each other. However, isotherms with the simulated data are a little less crowded in the Gulf Stream and Kuroshio regions than those with NOAAT. Correspondingly, northward flowing boundary

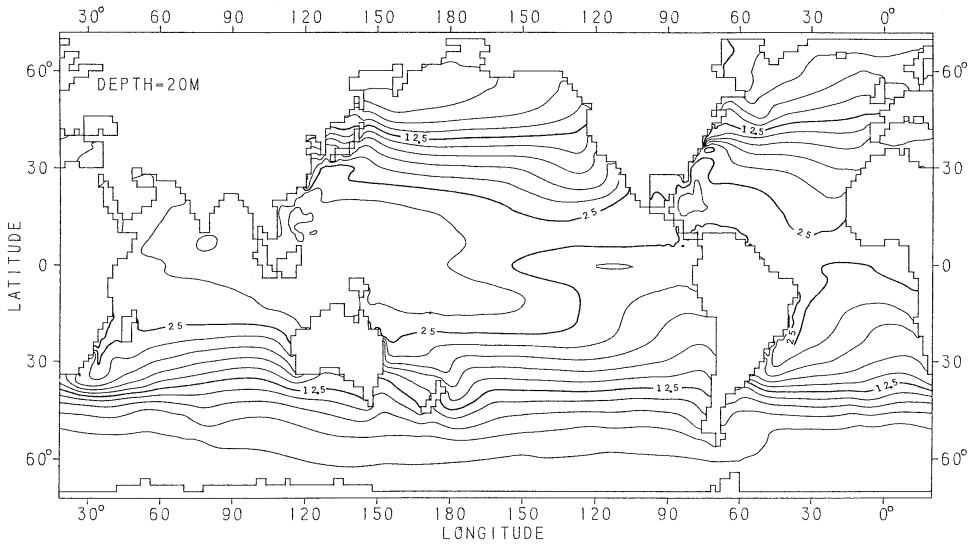


Fig. 2. Simulated sea surface temperature (°C). Annual average.

Table 2 Averages (°C) in the three oceans.

| depth(m) | Indian Ocean | | | | |
|---|---|---|---|---|---|
| | Case 1 | Case 2 | Case 3 | Case 4 | Obs |
| 20 | 17.24 | 17.24 | 18.20 | 18.12 | 18.24 |
| 280 | 9.30 | 10.30 | 11.64 | 12.19 | 10.25 |
| 720 | 4.68 | 5.06 | 6.04 | 7.57 | 6.81 |
| 1300 | 2.68 | 2.58 | 2.66 | 3.30 | 3.68 |
| 3100 | 1.85 | 1.73 | 1.66 | 1.76 | 1.44 |
| | Pacific Ocean | | | | |
| | Case 1 | Case 2 | Case 3 | Case 4 | Obs |
| 20 | 19.03 | 19.12 | 19.87 | 19.84 | 20.06 |
| 280 | 10.21 | 11.17 | 12.55 | 13.18 | 10.88 |
| 720 | 5.06 | 5.33 | 6.21 | 7.74 | 5.43 |
| 1300 | 3.02 | 3.02 | 3.20 | 3.71 | 3.15 |
| 3100 | 2.14 | 2.11 | 2.09 | 1.87 | 1.66 |
| | Atlantic Ocean | | | | |
| | Case 1 | Case 2 | Case 3 | Case 4 | Obs |
| 20 | 16.47 | 16.52 | 17.49 | 17.56 | 17.58 |
| 280 | 7.98 | 8.79 | 9.96 | 11.27 | 10.57 |
| 720 | 3.77 | 3.93 | 4.73 | 6.32 | 5.83 |
| 1300 | 2.41 | 2.37 | 2.66 | 3.65 | 3.81 |
| 3100 | 1.75 | 1.67 | 1.65 | 1.74 | 2.36 |

currents, Kuroshio and Gulf stream, go up far north, and southward flowing boundary currents, Oyashio and Labrador Current, poorly develop. The simulated SST is higher by about 2°C around the Antarctica and is a little lower in low latitudes. The simulated SST averaged over the whole ocean surface is very slightly lower than that of NOAAT. The simulated temperatures averaged over the individual ocean is shown in Table 2. The sixth column (Obs) gives averages of NOAAT at the surface, 275m (average of those at 250m and 300m depths), 700m, 1300m and 3000m depths, which are close to the depths of simulated temperatures. The differences between the three oceans are not well simulated. At 720m, 1300m and 3100m depths the average is highest in the Pacific Ocean and lowest in the Atlantic Ocean, while the average of NOAAT is highest in the Indian Ocean and lowest in the Pacific Ocean at 720m, highest in the Atlantic Ocean and lowest in the Pacific Ocean at 1300m, and highest in the Atlantic Ocean and lowest in the Indian Ocean at 3100m. These differences appear more distinctly in the longitudinal average. One of the striking differences in NOAAT between the Pacific and Atlantic Oceans is that, at 275m and 700m the Pacific Ocean temperature is much lower at northern mid-latitudes and much higher at southern mid-latitudes, and that, at 3000m the Pacific Ocean is colder at low- and mid-latitudes. At some latitudes, the simulated result agrees qualitatively with this observed result, but does not

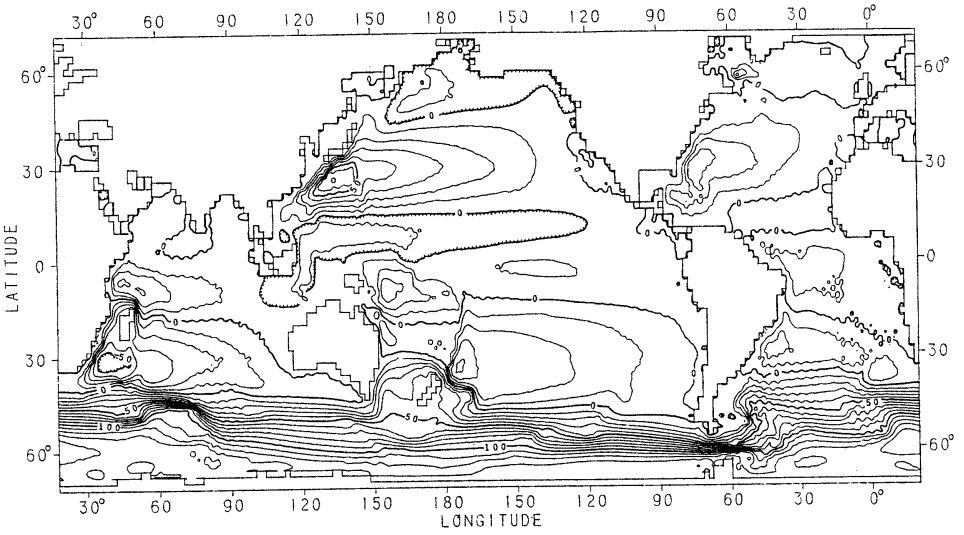


Fig. 3. Stream lines for the vertical integral of horizontal velocity (sv). Annual average.

agree quantitatively; the simulated difference between the two oceans is smaller.

A difference which is not remarkable in the annual maps but remarkable in monthly or seasonal maps is that isotherms by the simulated data are smooth (almost parallel to parallels) as in Fig.2, while those by NOAAT are wavy, in particular, south of 35°S in spring of the northern hemisphere.

Isotherms sharply push southward at and around the Mozambique Strait, which is related to the Agulhas Retroflection defined as a sharp anticyclonic turn of the Agulhas Current to the east at the Agulhas Bank near 22°E off the southern terminus of Africa.

In the Indian Ocean, isotherms north of the equator show different patterns, depending on the monsoon activity. In the southern hemisphere, however, the wind pattern does not vary much with time, so that the pattern of isotherms remains almost unchanged with time.

The incoming heat flux is calculated with Formula (1). Except in May and June, the monthly heat flux averaged over the whole ocean surface is downward. The annual average is downward and 7.8 W/m$^2$. If the global ocean is heated at this rate, its average temperature will increase by 0.014°C/year. However, the monthly maximum downward flux ranges from 188 to 475 W/m$^2$, and the monthly maximum upward flux ranges from 215 to 612 W/m$^2$. Both are much larger than the space and time average 7.8 W/m$^2$, suggesting that an almost steady state is reached statistically.

On the annual basis, a large amount of heat goes upward from the Kuroshio and Gulf Stream regions. The simulated outgoing and incoming fluxes are larger in magnitude in most regions than those by ESBENSEN and KUSHNIR (1981) based on climatological data, but there is no significant difference in the large scale pattern of isopleths between them. There is no significant difference, either, all the year round.

The longitudinal-annual average is also a little larger than that by observations (LAMBERT and BOER, 1989).

In spring there is almost no outgoing heat flux from the Kuroshio and Gulf Stream regions to the atmosphere. The heat flux is downward into these regions for a limited short period of summer.

## 4. Currents

Figure 3 shows the annual average of the barotropic component of velocity in terms of stream lines. Compared with common knowledge based on observations, the subtropical gyre develops too much to the north in the western North Pacific and North Atlantic Oceans. Its transport is 75.7sv in the former and 41.6sv in

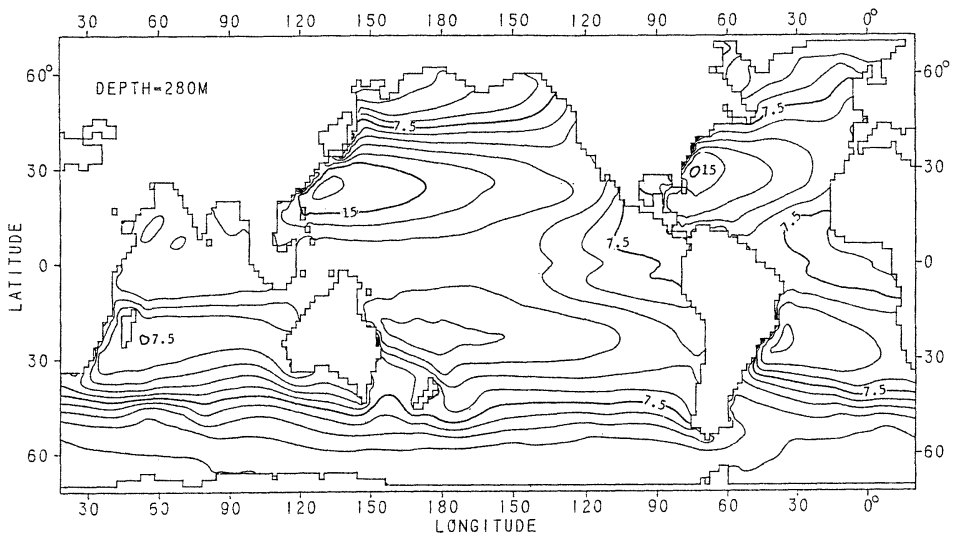


Fig. 4. Simulated temperature (°C) at a depth of 280m. Annual average.

the latter. The Oyashio and the Labrador Current poorly develop. In a simulation of the world ocean circulation by SEMTNER and CHERVIN (1988, 1992) with a fine grid of 0.5° ×0.5°, the subtropical gyre develops too much, too. This is also the case of a simulation of the North Pacific circulation by TAKANO and MISUMI (1990) with a grid of 1°×1°. Although many studies have been done on western boundary currents, mechanism of separation of them from the western boundary is still poorly understood (e.g., HAIDVOGEL *et al.*, 1992). These unrealistic features do not seem to be readily improved by increasing horizontal resolution.

In the North Pacific Ocean, the subarctic gyre transport ranges from 17sv in summer to 35 sv in winter, and the subtropical gyre transport ranges from 68 sv in summer to 82 sv in winter. In the North Atlantic Ocean, the subarctic gyre transport ranges from 31sv in summer to 37sv in early spring, and the subtropical gyre transport ranges from 37sv in late summer to 50 sv in winter. The annual variation is most prominent in the northern North Pacific Ocean.

The Agulhas Current clearly appears with 50 to 60 sv. Most of it does not go into the South Atlantic Ocean, but turns to the east after passing through the Mozambique Strait.

Importance of the Indonesian Throughflow (transport between Eurasia and Australia) in the global heat transport has been emphasized recently as a gateway of heat export from the Pacific Ocean to the Atlantic Ocean (GORDON, 1985, 1986). It does not apparently exist in the annual average transport, but does in summer months of the southern hemisphere to join the Madagascar Current through a current across the Indian Ocean which is hereafter referred to as "Orient Express" (or "Indian Ocean Express"). The Orient Express is distinctly traced by isotherms at a depth of 280m in Fig.4 (annual average) and throughout the year, and NOAAT also.

Figure 5 shows the annual variation of the transports of the Antarctic Circumpolar Current (transport through the Drake Passage), Kuroshio, Gulf Stream, Indonesian Throughflow and Agulhas Current in the four cases. The transports of the Kuroshio and Gulf Stream are tentatively defined as the maximum values of the stream function in the western boundary regions. The maximum value is located south of Honshu (Japanese mainland) in the Kuroshio region throughout the year, but its location in the Gulf Stream region changes with time within the range of about 600km. While the Kuroshio transport becomes minimum in September, the Gulf Stream transport shows two minima, March–April and September–October.

The transport of the Antarctic Circumpolar

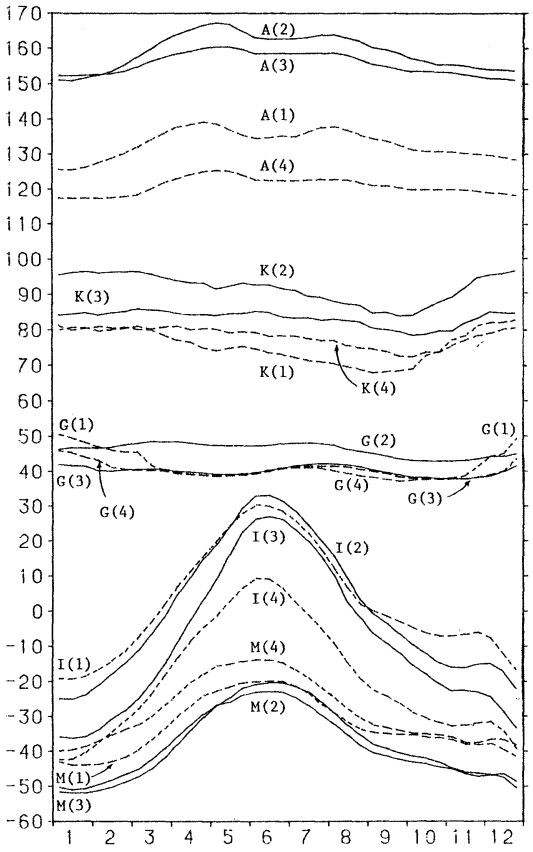


Fig. 5. Transports (sv) of the Antarctic Circumpolar Current (A), Kuroshio (K), Gulf Stream (G), Indonesian Throughflow (I) and Agulhas Current (M). Numbers 1 to 4 in parentheses refer to Cases 1 to 4.

Current at the Drake Passage ranges from 125sv in January to 139sv in May. An observation by REID and NOWLIN (1971) gives 235 sv as transport at the Drake Passage in January. CALLAHAN's result (1971) is similar to it, but FOSTER (1972) gives −15sv (westward transport). By analysis of data from heavily instrumented moorings and hydrographic cruises, WHITEWORTH (1983) shows that the total transport at the Drake Passage is probably between 118 sv and 146 sv. His result is very close to the transport simulated here, although the present study does not take sea ice into account and the coastline of the Antarctica is somewhat subjectively set up. It might be remarked that GILL and BRYAN (1971) point out the transport depends to a great extent on the geometry of the Antarctic Ocean. According to WHITEWORTH's result, the transport is small in December to January and seems to have two weak maxima, in July-August and in March-April. This also agrees with the simulated result.

In contrast to the Antarctic Circumpolar Current, the Indonesian Throughflow is not well simulated. Althouth no many reliable observational results are available, it seems to flow throughout the year from the Pacific Ocean to the Indian Ocean (GORDON, 1986; MURRAY and ADRIEF, 1988). Figure 5 indicates it flows from the Indian Ocean from April to August. The simulated annual range is about 50sv, which is probably too large. This discrepancy might result from poor resolution of the bottom topography near Greater and Lesser Sundas.

The transport of the Agulhas Current (value of the stream function along the coast of Madagascar) varies in phase of the Indonesian Throughflow; strong in winter and weak in summer.

In the other three cases, the pattern of the annual cycle is similar to that in Case 1, though the magnitude of the transport is different from each other.

It is noted, for comparison, that SEMTNER and CHERVIN (1992) gives 15 to 45sv to the Gulf Stream off Cape Hatteras, up to 200sv to the Kuroshio, about 200sv with oscillations of about 8sv to the Antarctic Circumpolar Current at the Drake Passage, about 70sv to the Agulhas Current with almost no seasonal cycle, and 12 to 22sv to the Indonesian Throughflow directed from the Pacific Ocean to the Indian Ocean throughout the year.

Figure 6 shows examples of the annual variation of the speed of the baroclinic component at the upper two layers at 135°E, 31°N (in the Kuroshio), 77°W, 29°N (in the Gulf Stream) and 43°E, 17°S (in the Agulhas Current).

Although the transport and barotropic component of velocity of the Kuroshio are strong in winter and weak in summer, its baroclinic component is strong in summer, and weak in fall. Similar annual variations are seen in the Gulf Stream. This phase difference between the barotropic and baroclinic components of velocity is shown also by TAKANO and MISUMI (1990). This is, however, not the case of the

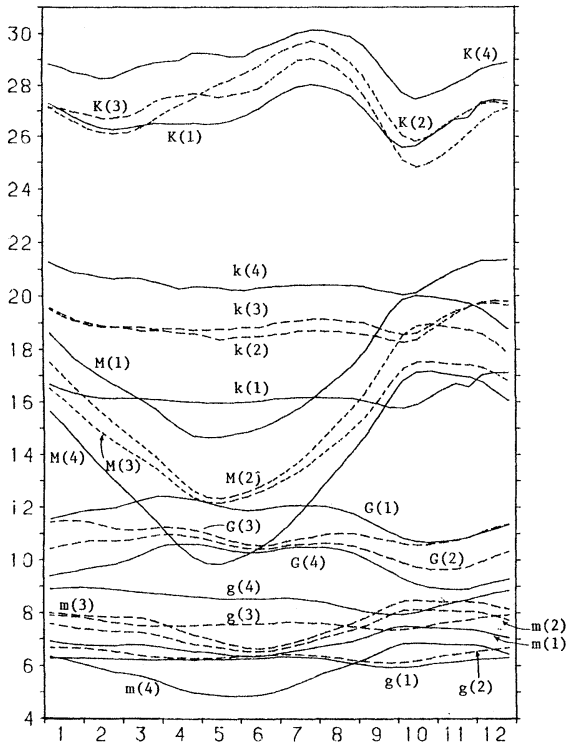


Fig. 6. Speed (cm/s) at the upper two layers in the Gulf Stream (G, g), Kuroshio (K, k) and Agulhas Current (M, m). Capitals refer to the first (surface) layer and small letters to the second layers. Numbers in parentheses refer to Cases 1 to 4, respectively.

Agulhas Current; both transport and baroclinic component at the upper two layers are strong in winter and weak in summer. The baroclinic component of the Indonesian Throughflow is directed to the Pacific Ocean at the upper two layers throughout the year, indicating importance of the barotropic component even at upper layers.

Figure 7 shows the annual average of surface currents (sum of the barotropic and baroclinic component). The scale is shown on the upper left. The maximum speed at the surface is 30 cm/s. The arrow length is proportional to the speed. Surface current pattern mostly agrees with the transport pattern shown in Fig.3. The Indonesian Throughflow which is not clear in Fig.3 flows into the Indian Ocean and goes to the west as the Orient Express. It is more clearly identified in summer months of the southern hemisphere.

The Indonesian Throughflow is directed to the Indian Ocean at a depth of 280m, directed rather to the Pacific Ocean at a depth of 760m, and clearly directed to the Pacific Ocean at a depth of 1300m. Both oceans are separated at the lowermost level 3100m deep.

A part of the Agulhas Current flows into the Atlantic Ocean through the upper two layers 500m thick over 220km (34°S to 36°S) at 21°E at a rate of 2.0 sv on the annual average. Between

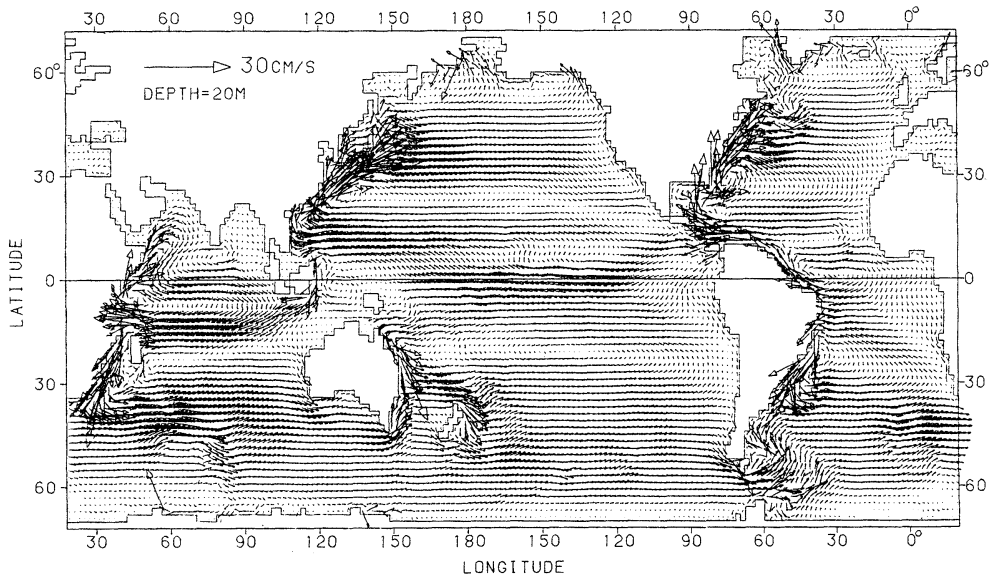


Fig. 7. Horizontal velocity vectors. Annual average. Scale on the upper left.

36°S to 38°S it flows westward at a rate of 4.2sv except at the surface layer with an eastward flow, so that the total westward transport is 6.2sv. This westward transport off the southern terminus of Africa is larger in summer than in winter of the southern hemisphere.

At the Drake Passage, the Antarctic Circumpolar Current extends from the surface to the bottom 2200m deep. Since the reference atmospheric temperture is a little lower in the Atlantic sector than in the Pacific sector of the Antarctic Ocean, the surface cooling should be stronger in the Atlantic sector, and Atlantic deep layers have trend toward cooling compared with Pacific deep layers. In fact, the simulated temperature is lower in Atlantic deep layers, though the simulated time of integration may not be enough for deep layers to reach a complete equilibrium state.

The vertical component of velocity, either upward or downward, is strong at the equator and by the borderline between land and water. A strong downwelling area is located southeast of Madagascar at 500m depth, which is closely related to the presence of simulated and observed subsurface warm water masses.

The meridional overturning (meridional circulation) is of importance in the meridional heat transport. The vertical and northward components of velocity are integrated over the latitude arc for defining the stream function for the meridional overturning. On the annual average, the maximum value is 47sv in the southern hemisphere, and 30sv in the northern hemisphere. It might be remarked that these figures do not necessarily mean the intensity of large scale sinking from the high latitude surface in the both hemispheres, but only a measure of the overall vertical motion. On the annual cycle, the maximum sinking rate in the southern hemisphere ranges from 46sv in October to 97sv in December, and 28sv in September to 86sv in December in the northern hemisphere.

## 5. Concluding remarks

The present study is successful in simulating major large scale features of the general circulation in the world ocean: sea surface temperature, transport of the Antarctic Circumpolar Current at the Drake Passage, Agulhas Retroflection and Orient Epress.

The Oyashio and Labrador Current poorly develop in association with overdeveloped subtropical gyres in the Pacific and Atlantic Oceans. Some important processes might be missing in the model for the separation of the northward current from the western boundary and the development of the subarctic gyres.

Salinity and sea ice should be of some importance. It is remarked, however, that a model with salinity as a prognostic variable is not successful, either, in simulating the Oyashio and Labrador Current (SEMTNER and CHERVIN, 1988, 1992; TAKANO, 1992b).

The grid size is larger than 1° in most of the global ocean models so far used. In the present study it is not fine enough, either, to resolve the mesoscale eddies. Although their role is not yet clearly understood, the meridional heat transport in the numerical model seems to be almost independent of it, provided that the grid size is smaller than 1° or 2° (TAKANO, 1982).

## References

ARAKAWA, C. and K. TAKANO (1991): Oceanic angular momentum estimated with a general circulation model. La mer, **29**, 52–56.

CALLAHAN, J. E. (1971): Velocity structure and flux of the Antarctic Circumpolar Current south of Australia. J. G. R., **76**, 5859–5864.

ESBENSEN, S. K. and V. KUSHNIR (1981): The heat budget of the global ocean. An atlas based on estimates from surface marine observations. Clim. Res. Ins., Rep. No. 29., Oregon State Univ., 27pp., 188 figs.

FOSTER, L. A. (1972): Current measurements in the Drake Passagee. MSc thesis, Dept. Oceanogr., Dalhousie Univ.

FRIEDRICH, H. and S. LEVITUS (1972): An approximation to the equation of state for sea water, suitable for numerical ocean models. J. Phys. Oceanogr., **2**, 514–517.

GILL, A. E. and K. BRYAN (1971): Effects of geometry on the circulation of a three-dimensional southern hemisphere ocean model. Deep-Sea Res., **18**, 51–64.

GORDON, A. L. (1985): Indian-Atlantic transfer of thermocline water at the Agulhas Retroflection. Science, **227**, 1030–1033.

GORDON, A. L. (1986): Interocean exchange of thermocline water. J. G. R., **91**, 5037–5046.

HAIDVOGEL, D. B., J. C. McWILLIAMS and P. R.

GENT (1992): Boundary current separation in a quasigeostrophic, eddy-resolving ocean circulation model. J. Phys. Oceanogr., **22**, 882–902.
HELLERMAN, S. and M. ROSENSTEIN (1983): Normal monthly wind stress over the world ocean with error estimates. J. Phys. Oceanogr., **13**, 1093–1104.
LAMBERT, S. J. and BOER, G. J (1989): Atmosphere-ocean heat fluxes and stress in general circulation models. Atmos.-Ocean, **27**, 692–715.
MURRAY, S.P. and D. ARIEF (1988): Throughflow into the Indian Ocean through the Lombok Strait, January 1985–January 1986. Nature, **333**, 444–447.
National Geophysical Data Center (1986): Worldwide gridded bathymetry–DBDB5.
NODC (National Oceanographic Data Center) / NOAA (1983) : Climatological atlas of the world ocean, annual and seasonal analyses. NOAA, Washington, D. C., USA.
REID, J.L. and W.D. NOWLIN (1971): Transport of water through the Drake Passage. Deep-Sea Res., **18**, 51–64.
SEMTNER, A. J. and R. M. CHERVIN (1988): A simulation of the global ocean circulation with resolved eddies. J. G. R., **93**, 15502–15522.
SEMTNER, A. J. and R. M. CHERVIN (1992): Ocean general circulation from a global eddy-resolving model. J.G.R., **97**(C), 5493–5550.
TAKANO, K. (1974): A general circulation model for the world ocean. Tech. Rept. No. 8, Num. simul. weather and climate, Dept. meteorol., Univ. Calif., Los Angels, 46pp.
TAKANO, K. (1975): Relationship between the grid size and the coefficients of lateral eddy viscosity in the finite difference computation of the linear vorticity equation in the oceans. J. Oceanogr. Soc. Japan, **31**, 105–108.
TAKANO, K. (1982): Grid-size dependency of the meridional heat transport in a numerical model of an ocean. Atmos.-Ocean, **20**, 258-267.
TAKANO, K. (1986): An ocean model. Rept. Preoper. Survey for Ocean Dump. Radioactive Wastes. Radioactive Wastes Manag. Center, Tokyo, 270pp. (in Japanese)
TAKANO, K. (1992a): Sea surface height calculated with a rigid-lid world ocean circulation model. Proc. CEG/IVth ISC, China Meteorol. Press, Beijing 155–165.
TAKANO, K. (1992b): Kuroshio power estimate with a general circulation model. Proc. Symp. China-Japan Joint Res. Prog. on the Kuroshio, Qingdao (in press).
TAKANO, K. and A. Misumi (1990): Numerical simulation of the North Pacific circulation as a fundamental study on the Kuroshio power harnessing. Proc. Japan-China Joint Res., STA (Japan) and SOA (China), 146–156.
WHITEWORTH, T. III (1983): Monitoring the transport of the Antarctic Circumpolar Current at Drake Passage. J. Phys. Oceanogr., **13**, 2045–2057.

# 世界じゅうの海水の大循環の数値シミュレーション
## 第1部　水温と流速の分布

新川千歳世・高野健三

**要旨**：海が1年を通じて緯度線を横切って南北方向に運ぶ熱量、、および，となりの海との間をゆききする熱量を海洋大循環モデルを使って求める。南緯70°から北緯70°まで緯度・経度とも2°ごとに格子点をおく。北極海を除く。氷と塩分を無視する。鉛直方向には5層を設ける。海水は海面での（鉛直）熱流量と風の応力によって駆動される。第1部では水温と流速の分布を示す。格子が粗いので細かい特徴を再現できないが，大規模特徴は観測結果とだいたい一致する。南極海流の流量は妥当であるが，黒潮や湾流は北に延びすぎるし，インドネシア通り抜け（Indonesian Throughflow）は，（南半球の）夏にはインド洋から太平洋に向かい，観測結果と一致しないようである。この流れに始まるオリエント急行（インド洋特急ともいう）は水温・流速・（流量についての）流線の分布に現れる。その末端の一部は，アフリカの南端をまわって大西洋に入る。第2部では熱輸送について述べる。